Angle-domain common image gathers by wave-equation migration

Marie L. Prucha* and Biondo L. Biondi, Stanford University, William W. Symes, Rice University

SUMMARY

Shot- and offset-domain common image gathers encounter problems in complex media. They can place events that come from different points in the subsurface at one subsurface location based on identical arrival times and horizontal slownesses. Angle-domain common image gathers uniquely define ray couples for each point in the subsurface, therefore each event in the data will be associated with only one subsurface location. It is possible to generate angle-domain common image gathers with wave-equation migration methods and these angle-domain common image gathers may be used for velocity analysis and amplitude-versus-angle analysis.

INTRODUCTION

Current depth imaging technology works very well in areas that have slow velocity variations but may fail in more complex areas (Claerbout, 1985) for a variety of reasons, such as multiple reflections, bad velocities, and spatial aliasing. One potential cause of imaging failure is reflector location ambiguity due to multipathing of reflected energy: it is possible that a single event recorded in the data at one surface location could come from reflectors at two or more subsurface locations. Besides contributing to imaging artifacts, reflector ambiguity contributes non-flat events to common image gathers, thus rendering velocity analysis ambiguous (Nolan and Symes, 1996).

Several authors have suggested *angle domain* imaging as a solution for the reflector ambiguity (Xu et al., 1998; Brandsberg-Dahl et al., 1999). Angle domain sections collect the energy in a data set which has scattered over a specific reflection ("opening") angle θ. We will argue below that an event in an angle section uniquely determines a ray couple, which in turn uniquely locates the reflector. Thus imaging artifacts and velocity update ambiguity due to multipathing are eliminated in this domain.

Multipathing is better handled by wave-equation migration methods than Kirchhoff ones, therefore the former are a natural choice for producing angle-domain common image gathers (CIGs). We present a simple method for extracting CIGs from 3-D prestack data downward continued using the Double Square Root equation (DSR). The method is based on a slant-stack decomposition of the downward continued wavefield at each *depth* level. Our method is thus different from the method proposed by Ottolini and Claerbout (1984), that applies the DSR to downward continue prestack data slant-stacked at the *surface*. In layered media the two methods should produce equivalent results, but in presence of lateral velocity variations plane-wave downward continuation is not strictly valid and true angle-domain CIGs can only be produced by wavefield decomposition at depth.

Migration methods based on DSR operators have been applied to 2-D prestack migration for long time (Claerbout, 1985). However, the direct application of DSR migration methods to 3-D prestack data have been prevented by the tremendous computational cost. Only recently computationally efficient methods to continue 3-D prestack data have been presented (Biondi and Palacharla, 1996; Mosher et al., 1997). In particular, common-azimuth migration is an attractive alternative to Kirchhoff migration for sub-salt imaging because of its robustness with respect to the complex multipathing that is induced by salt bodies.

This abstract will explain how some widely used common image gathers can contain reflector ambiguity due to multipathing and why angle domain common image gathers will not. Then we will demonstrate the construction of angle-domain common image gathers from wave equation downward continued data for use in velocity analysis and amplitude-versus-reflection angle analysis.

KINEMATICS OF MULTIARRIVALS IN THE SHOT AND OFFSET DOMAINS

The kinematics of shot domain common image gathers and offset domain image gathers are well understood in constant velocity and $v(z)$ media. Difficulties arise when we begin considering complex subsurfaces with rapid lateral velocity variations. Even in 2-D it is easy to construct a model for which an individual common shot gather or common offset gather can contain two events from two points in the subsurface that arrive at the same time and are indistinguishable. Let us investigate particular cases of these occurrences.

An individual common shot gather is parameterized by the receiver location r. If two raypaths between the same source and receiver exist such that they have the same receiver horizontal slowness p_r and the two-way traveltime along each is the same, it is impossible to distinguish between the two reflector locations (Nolan and Symes, 1996). Figure 1 shows a very simple case of this.
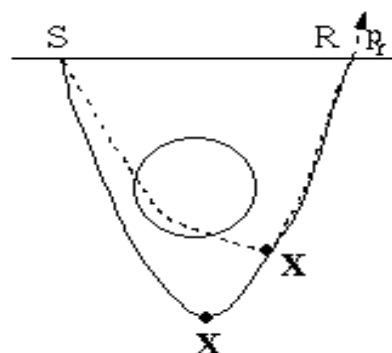

Figure 1: Individual shot gather: the circular lens is a low velocity anomaly so the traveltimes and p_r are identical.

An individual common offset gather is parameterized by midpoint m. Suppose that the horizontal midpoint slowness $p_m = p_s + p_r$ is the same for two raypaths with the same traveltimes. Once again, the two raypaths represent the same event, and the location of the reflector causing this event is completely ambiguous. Figure 2 shows a case where $p_{s1} = -p_{r1}$ and $p_{s2} = -p_{r2}$ so that $p_{m1} = p_{m2} = 0$.

By shooting a fan for rays from both **x** locations in Figure 2, it is possible to obtain traveltime curves for a common offset. These curves are shown in Figure 2. The traveltime curve for the diffractor inside the anomaly is nicely hyperbolic. The curve for the deeper diffractor is discontinuous due to the shadow zones that occur above the edges of the anomaly but the symmetrical triplications can be seen. At this offset, the traveltimes for both curves are identical for the midpoint directly above the diffractors. From the geometry of the model, it is clear that the midpoint slownesses are the same, therefore the events in the data will be indistinguishable.

KINEMATICS OF MULTIARRIVALS IN THE ANGLE DOMAIN

We confine our discussion to the 2D case; the 3D case is similar, provided that complete surface coverage is available. Specular reflection connects a *reflector element*, consisting of a subsurface position
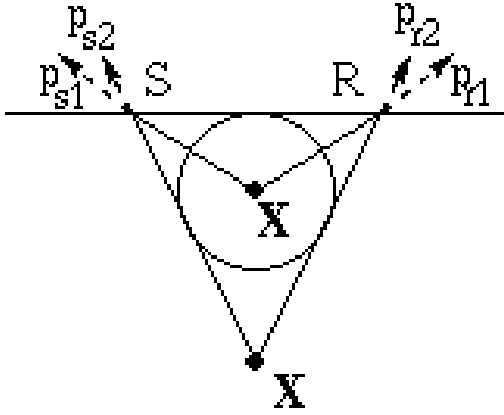
Figure 2: Individual offset gather: the circular lens is a low velocity anomaly so the traveltimes are identical and the midpoint slownesses are equal.
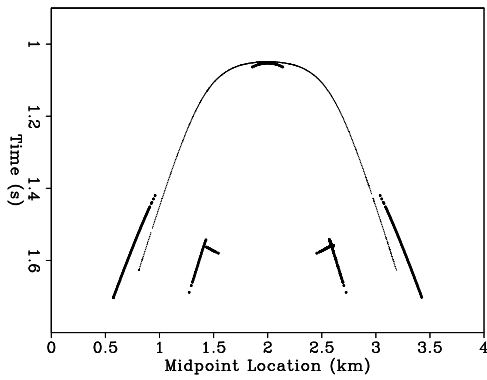

Figure 3: Traveltime curves for the model in Figure 2. The thick curve is for the deeper reflector and is discontinuous due to shadow zones.
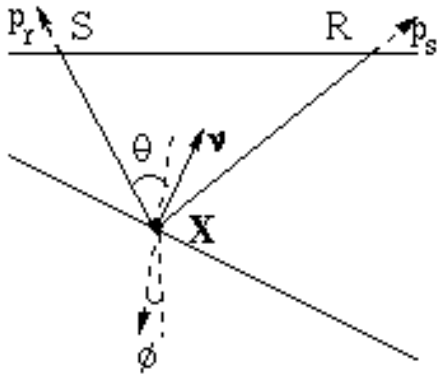

Figure 4: Simple reflection: the vector ν is normal to the reflector, θ is one-half the reflection angle, and ϕ is related to the dip angle.

$\mathbf{x}$ containing the midpoint location $\mathbf{m}$ and the depth z and *dip vector* ν representing the reflector normal at that position with an *event element* s, p_x, r, p_r, t consisting of source and receiver positions s and r, source and receiver horizontal slownesses p_s and p_r, and two way time t. The connection *via* incident and reflected rays is depicted in Figure 4, which also shows the *opening angle* θ.

Note that given $\mathbf{x}$, ν, and θ, the incident and reflected rays and the event element s, p_s, r, p_r, t are completely determined: therefore the latter are functions of $\mathbf{x}$, ν, and θ.

The angle transform of a data set $\{d(s, r, t)\}$ is

$$a(\mathbf{x}, \theta) = \int \int d\nu w(\nu, \theta, \mathbf{x}) d(s, r, t)$$

The principle of stationary phase shows that an event in a single angle panel, i.e. a position $\mathbf{y}$ and an *angle domain dip vector* η, arise when incident and reflected rays meet at $\mathbf{y}$ and are bisected by η; these rays determine once again an event element s, p_s, r, p_r, t, *and this event must have been present in the data for the event in question to be present in the angle domain.* Of course the event element s, p_s, r, p_r, t completely determines the rays in the subsurface carrying the energy of the event. We assume the *Traveltime Injectivity Condition* (ten Kroode et al.,): a pair of rays and a total (two-way) time determines at most one reflector element. In that case, the event in the angle domain is compatible with at most one reflector element.

Note the contrast with the constant offset domain as described in the preceding section where an event element in the data could correspond kinematically to more than one reflector element.

The velocity field used to generate the rays used in the formation of the angle transform does not necessarily need to be the same as the velocity field which gave rise to the moveout in the data - which is fortunate, as we don't know the latter at the outset of the migration / velocity analysis process, and have only an approximation of it at the end! When the two velocity fields are different, the angle transform events will not necessarily match the reflectors in the Earth: the two will differ by a residual migration. When the two velocity fields are the same, the image is perfect, i.e. $(\mathbf{x}, \nu) = (\mathbf{y}, \eta)$.

ANGLE-DOMAIN CIG BY WAVE-EQUATION MIGRATION

In the previous sections we discussed the advantages of angle-domain CIGs over offset-domain CIGs when a complex velocity function induces multipathing and event triplication. In this section we show how to extract angle-domain CIGs from downward-continued prestack data.

Recorded 3-D seismic data can be organized as a function of midpoint coordinates ($\mathbf{m}$) and offset coordinates ($\mathbf{h}$). Prestack data are efficiently downward continued using the DSR equation in the frequency (ω) domain. Furthermore, since we either use 2-D downward continuation or 3-D common-azimuth downward continuation, the offset space is restricted to the in-line offset h_x, and thus we express the recorded wavefield as $P(\omega, \mathbf{m}, h_x; z = 0)$, where z is depth and z=0 indicates data recorded at the surface.

The prestack wavefield at depth is obtained by downward continuing the recorded data using the DSR, and is imaged by extracting the values at zero time

$$P(\omega, \mathbf{m}, h_x; z = 0) \quad \stackrel{DSR}{\Longrightarrow} \quad P(\omega, \mathbf{m}, h_x; z) \quad (1)$$

$$P(\omega, \mathbf{m}, h_x; z) \quad \stackrel{Imaging}{\Longrightarrow} \quad P(t = 0, \mathbf{m}, h_x; z) \quad (2)$$

The downward-continuation process focuses the wavefield towards zero offset (left panel in Figure 5) and if the continuation velocity is correct, a migrated image can be obtained by extracting the value of the wavefield at zero offset. However, the zero-offset wavefield has

Offset domain

Offset (km)
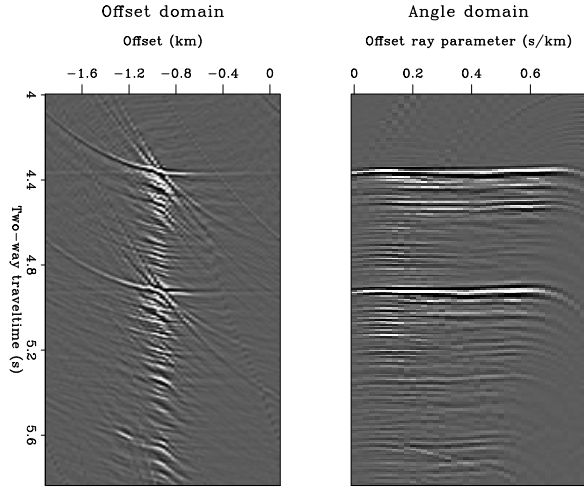

Angle domain

Offset ray parameter (s/km)

Figure 5: Left: Offset panel after downward continuation. Right: Angle-domain CIG

Correct velocity

Offset ray parameter (s/m)

Constant velocity

Offset ray parameter (s/m)

Figure 6: Left: Angle-domain CIG with correct velocity. Right: Angle-domain CIG with too low constant velocity.

limited diagnostic information for velocity updating, and no information on the amplitude of the reflections versus reflection angle (AVA). We therefore perform a slant stack along the offset axis before imaging and obtain an image as a function of the offset ray parameter p_{hx}, as

$$P(\omega, \mathbf{m}, h_x; z = 0) \quad \overset{DSR}{\Longrightarrow} \quad P(\omega, \mathbf{m}, h_x; z) \tag{3}$$

$$P(\omega, \mathbf{m}, h_x; z) \quad \overset{Slant\ stack}{\Longrightarrow} \quad P(\tau, \mathbf{m}, p_{hx}; z) \tag{4}$$

$$P(\tau, \mathbf{m}, p_{hx}; z) \quad \overset{Imaging}{\Longrightarrow} \quad P(\tau = 0, \mathbf{m}, p_{hx}; z). \tag{5}$$

$$\tag{6}$$

Angle-domain CIGs are subsets of $P(\tau = 0, \mathbf{m}, p_{hx}; z)$ at fixed midpoint location. The right panel in Figure 5 shows the angle-domain CIG gather corresponding to the downward-continued offset gather shown in the left panel. Notice that because in downward-continued offset gathers the energy is concentrated around zero offset, the slant stack decomposition does not suffer from the usual artifacts caused by the boundary conditions.

Strictly speaking, the CIG gathers obtained by the proposed procedure are function of the offset ray parameters p_{hx} and not of the aperture angle θ. However, p_{hx} is linked to θ by the following simple trigonometric relationship

$$p_{hx} = \frac{2 \sin \theta \cos \phi}{V(z, \mathbf{m})}, \tag{7}$$

where ϕ is the geological dip along the in-line direction and $V(z, \mathbf{m})$ is the velocity function.

Angle-domain CIG and velocity
Angle-domain CIGs can be used to update the velocity function after migration similarly to the way that offset-domain CIGs are currently used (Brandsberg-Dahl et al., 1999) or for wave-equation Migration Velocity Analysis (Biondi and Sava, 1999). As for offset-domain CIGs, if the velocity function is correct the reflections are aligned along the angle axis. If the velocity function is too low the reflections will smile upward; if the velocity function is too high the reflections will frown downward. This behavior is demonstrated by the analysis of the gathers in Figure 6. The gathers were extracted from a 3-D prestack wavefield focused using common-azimuth downward continuation. The left gather was obtained using the correct velocity. The right gather was obtained using a low constant velocity. Figure 7 shows the inline migrated section that passes through the gather shown in Figure 6. Notice that the CIG gathers show only the first kilometer of the image.
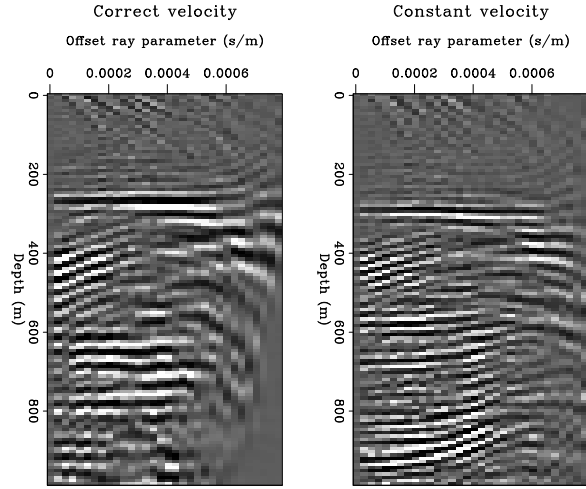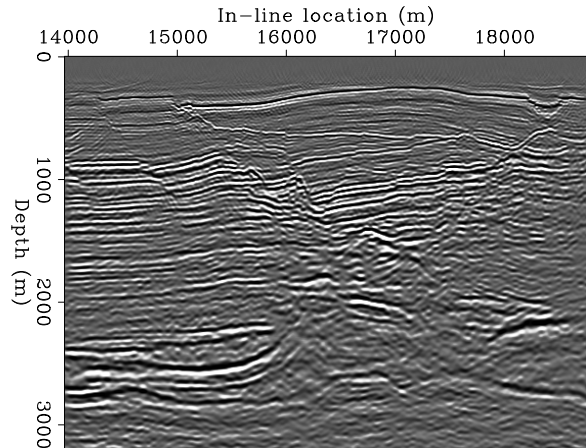
In-line location (m)

Figure 7: In-line section of 3-D migrated cube
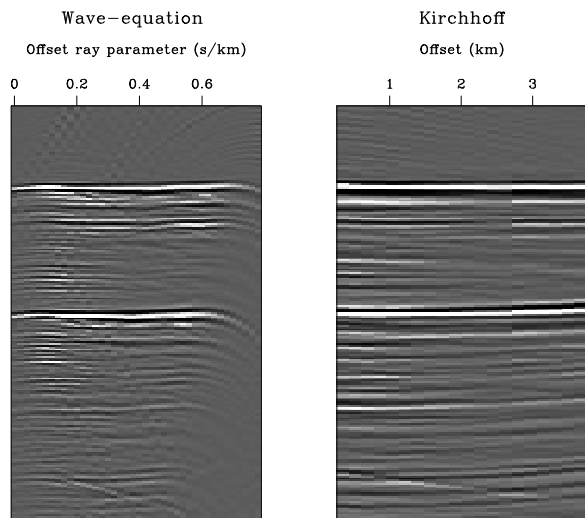
Reflection angle gathers

Figure 8: Right: Angle-domain CIG obtain by wave-equation migration. Left: Offset-domain CIG gather obtained by Kirchhoff migration

Angle-domain CIG and AVA

Angle-domain CIG can also be used to analyze the reflectivity as a function of the reflection angle to estimate rock and fluid properties in the subsurface. This potential use is illustrated by the gathers shown in Figure 8. The left panel shows an angle-domain CIG gather while the right panel shows the corresponding offset-domain CIG gather obtained by an amplitude preserving Kirchhoff migration (Ecker et al., 1996). The amplitude behavior as a function of offset ray parameter (left panel) is in qualitative agreement with the the amplitude behavior as a function of offset (right panel).

CONCLUSIONS

Angle-domain CIG gathers have attractive properties when a complex velocity model causes multipathing of reflected energy. They are free of the imaging artifacts caused by reflector-position ambiguity that degrade the image obtained from either shot gathers or common-offset gathers. We presented a simple method for extracting angle-domain CIGs from the prestack wavefield downward-continued using the wave equation. Our method produces high-quality CIG gathers that can be readily used for either velocity analysis or AVA analysis.

REFERENCES

Biondi, B., and Palacharla, G., 1996, 3-D prestack migration of common-azimuth data: Geophysics, **61**, 1822–1832.

Biondi, B., and Sava, P., 1999, Wave-equation migration velocity analysis: 69th Annual Internat. Mtg., Soc. Expl. Geophys., Expanded Abstracts, submitted.

Brandsberg-Dahl, S., de Hoop, M. V., and Ursin, B., 1999, Sensitivity transform in the common scattering-angle/azimuth domain: EAGE 61st Annual Conference, Expanded Abstracts, submitted.

Claerbout, J. F., 1985, Imaging the Earth's Interior: Blackwell Scientific Publications.

Ecker, C., Dvorkin, J., and Nur, A., 1996, Sediments with gas hydrates: Internal structure from seismic avo: 67th Annual Internat. Mtg., Soc. Expl. Geophys., Expanded Abstracts, 1767–1770.

Mosher, C. C., Foster, D. J., and Hassanzadeh, S., 1997, Common angle imaging with offset plane waves: 67th Annual Internat. Mtg., Soc. Expl. Geophys., Expanded Abstracts, 1379–1382.

Nolan, C. J., and Symes, W. W., 1996, Imaging and conherency in complex structure: Proc. 66th Annual International Meeting, 359–363.

Ottolini, R., and Claerbout, J. F., 1984, The migration of common-midpoint slant stacks: Geophysics, **49**, no. 03, 237–249.

ten Kroode, A. P. E., Smit, D.-J., and Verdel, A. R., Linearized inverse scattering in the presence of caustics: Wave Motion.

Xu, S., Chauris, H., Lambare, G., and Noble, M., 1998, Common angle image gather - a strategy for imaging complex media: Depth Imaging of Reservoir Attributes, X012.